Exploiting angular momentum to enhance bipedal center-of-mass control

Citation: Hofmann, A., M. Popovic, and H. Herr. "Exploiting angular momentum to enhance bipedal center-of-mass control." Robotics and Automation, 2009. ICRA '09. IEEE International Conference on. 2009. 4423-4429. ©2009 Institute of Electrical and Electronics Engineers.

As Published: http://dx.doi.org/10.1109/ROBOT.2009.5152573

Publisher: Institute of Electrical and Electronics Engineers

Persistent URL: http://hdl.handle.net/1721.1/59380

Version: Final published version: final published article, as it appeared in a journal, conference proceedings, or other formally published context

2009 IEEE International Conference on Robotics and Automation
Kobe International Conference Center
Kobe, Japan, May 12-17, 2009

Exploiting Angular Momentum to Enhance Bipedal Center-of-Mass Control

Andreas Hofmann, Marko Popovic and Hugh Herr

Abstract— **Recent humanoid control investigations have emphasized the importance of controlling whole-body angular momentum throughout a movement task. For typical movement tasks, such as normal walking, such controllers minimize fluctuations in angular momentum about the center of mass (CM). This minimization is consistent with observed behavior of humans for such tasks. However, there are cases where such minimization is not desirable. In this study, we investigate movement tasks where bipedal balance control requires a relaxation of the goal of minimizing whole-body angular moment. We construct a humanoid model having a human-like mass distribution, and a Moment-Exploiting Control algorithm that modulates whole-body angular momentum to enhance CM control. The model only requires reference trajectories for CM position and torso orientation. Joint reference trajectories are not required. While balancing on one leg, we show that the controller is capable of correcting errors in CM state by sacrificing angular postural goals for the swing leg, trunk and head. This prioritization capability provides robustness to significant disturbances, without the need to plan new reference trajectories. We compare the dynamic behavior of our humanoid model to that of human test participants. While standing on one leg, the model, like the human, is shown to reposition its CM just above the stance foot from an initial body state where CM velocity is zero, and the ground CM projection falls outside the foot envelope.**

I. INTRODUCTION

Over the past decade many impressive humanoid robots have been demonstrated that successfully walk on level unobstructed terrain [1]-[4]. The balancing of these robots is obtained using a control design that requires the machine to accurately track precisely calculated joint reference trajectories. Specifically, the robots use a referential *Zero Moment Point* (ZMP) planning approach in which joint reference trajectories are generated in advance based on a desired reference trajectory for the ZMP [5], and on other goals such as keeping the torso in a vertical upright posture. A limitation of this approach, particularly for irregular terrain ambulation, is that it is valid only in a close neighborhood of the reference trajectories; a significant disturbance requires real-time re-planning of the reference trajectories in order to maintain balance.

As a resolution to this difficulty, researchers [6] - [7], [9] used a simplified, inverted-pendulum model to generate compatible *Center of Mass* (CM) and ZMP trajectories at runtime, and then employed Jacobian relations to transform CM velocities into corresponding joint velocities. In a related approach [10] - [13] a resolved momentum controller directly regulates the linear momentum of the CM, and angular momentum about the CM. Related approaches [14] - [15] use cooperative lower and upper body motions to minimize whole-body angular momentum and CM moment. For example, they use trunk twisting and arm swaying to compensate for moment generated about the vertical axis due to movement of the swing leg.

The resolved momentum controllers [10] - [13] follow reference trajectories expressed in terms of linear momentum of the CM, and angular momentum about the CM. The reference trajectories for angular momentum are normally set to 0 for typical movement tasks. Significant angular momentum can be generated by these controllers, but only by specifying a significant reference trajectory for this.

The goal of minimizing angular momentum is reasonable in some circumstances; recent evidence shows that whole-body angular momentum remains small during steady-state human walking [16], [17]. However, a bipedal controller that strictly minimizes angular momentum may be problematic in some situations. By significantly varying whole-body angular momentum, humans modulate CM force to increase maneuverability and balance [17], [18].

In recent years, there has been an increasing recognition of the fact that bipedal locomotion is a multi-variable control problem where the control objectives can be in conflict; the system becomes over-constrained. Recent whole-body controllers [23], [19] automatically prioritize goals when they are in conflict. In particular, they are able to purposely depart from lower-priority components of their input reference trajectories in order to satisfy the higher-priority components. The advantage of this approach is that the resulting system is robust to significant disturbances, without the need for re-planning reference trajectories. One technique for prioritizing is to use quadratic programming, where the cost function is used to prioritize goals. An interesting example of this approach resulted in a balancing system that automatically generated arm rotation angular momentum to reject disturbances [26].

The Moment-Exploiting Control (MEC) algorithm described here is an example of such a prioritizing controller. It uses its prioritization capabilities to (when necessary) purposefully generate angular moment in order to augment the forces that can be applied to a robot's CM [18] - [20]. In this strategy both zero-moment CM force contributions,

A. Hofmann is Director of Machine Learning Research and Development at Vecna Technologies, Cambridge, MA, USA ahofmann@vecna.com

M.Popovic is with the MIT Media Laboratory, Massachusetts Institute of Technology, Cambridge, MA, USA marko@media.mit.edu

H. Herr is with the MIT Media Laboratory and the MIT-Harvard Division of Health Sciences and Technology, Massachusetts Institute of Technology, Cambridge, MA, USA hherr@media.mit.edu

as well as non-zero moment CM force contributions are exploited to increase CM positional control [21]. The MEC was previously evaluated on a simple three-link model [18], and additionally on an 18 degree-of-freedom, 3-dimensional simulated humanoid [19], [20]. For single-leg balancing, these models are capable of repositioning the CM just above the stance foot from an initial body state where CM velocity is zero, and the ground CM projection is outside the foot support envelope. Such a balancing feature is readily observed in humans but cannot be achieved using previous bipedal control schemes without significant replanning of the reference trajectories.

In this investigation, we further develop the MEC algorithm on a 3-dimensional simulated humanoid with human-like mass distribution and degrees of freedom. The capacity of the model to effectively exploit angular momentum to increase CM control is evaluated. In order to validate the model, and further investigate how humans exploit angular momentum, we compare our model's dynamical behaviors with those of human test participants. We compare in terms of the *Centroidal Moment Pivot* (CMP) [21], a recently developed ground reference point that is used to characterize whole-body rotational behaviors.

II. Background

Vukobratovic and Stepanenko defined the ZMP as the point of resulting reaction forces at the contact surface between the extremity and the ground [5]. We designate the horizontal axes as x and y, where x represents the anterior-posterior direction (front-back), and y the medio-lateral direction (left-right). The z axis is directed vertically. The position of the ZMP along the horizontal axes, x_{ZMP} and y_{ZMP} can be expressed in terms of CM position, force, and moment as

$$x_{ZMP} = x_{CM} - \frac{F_{grx}}{F_{grz}} z_{CM} - \frac{\tau_y}{F_{grz}}$$
$$y_{ZMP} = y_{CM} - \frac{F_{gry}}{F_{grz}} z_{CM} + \frac{\tau_x}{F_{grz}} \quad (1)$$

where x_{CM}, y_{CM}, and z_{CM} are the x, y, and z positions of the CM, F_{grx}, F_{gry}, and F_{grz} are the ground reaction forces in the x, y, and z directions, and τ_x and τ_y are the CM moments about the x and y axes, respectively [21]. The ZMP is always within the support base defined by the set of points in contact with the ground surface.

The Centroidal Moment Pivot (CMP) [16], [21] is that point on the ground, not necessarily within the support base, from which the ground reaction force vector would have to act in order to generate no moment about the whole-body CM (for τ_x and τ_y in 1 to be zero). Thus, it is that point where a line parallel to the ground reaction force vector, passing through the CM, intersects with the ground, as shown in Fig. 1B. The CMP can be expressed as

$$x_{CMP} = x_{CM} - \frac{F_{grx}}{F_{grz}} z_{CM}, y_{CMP} = y_{CM} - \frac{F_{gry}}{F_{grz}} \quad (2)$$

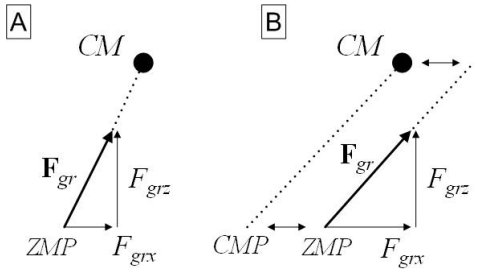

Fig. 1. In A) when no moment acts about the CM, the ground reaction force points from the ZMP to the CM position. When a non-zero moment acts as shown in B), the ZMP and CMP diverge.

By combining 1 and 2, we obtain a relation between ZMP and CMP, or

$$x_{CMP} = x_{ZMP} + \frac{\tau_y}{F_{grz}}, y_{CMP} = y_{ZMP} - \frac{\tau_x}{F_{grz}} \quad (3)$$

Equation 3 shows that when there is no horizontal moment about the CM, the CMP and ZMP points coincide. In this case, the ground reaction force vector points directly to the CM, as shown in Fig. 1A. Conversely, when there is a horizontal moment about the CM, the CMP and ZMP diverge. Note that as the CMP and ZMP diverge, the ZMP must remain within the support base, but the CMP may leave the region of support.

Horizontal ground reaction forces can be separated into zero-moment and moment components in 1 [21]. We call a strategy that uses the zero-moment force component a zero-moment strategy, and a strategy that uses the moment force component a moment strategy.

III. Methods

The MEC is a humanoid control architecture that focuses on the problem of exerting a horizontal force on the CM to redirect the CM towards a desirable state. The controller accomplishes this CM control using a combination of zero-moment and moment strategies. The zero-moment strategy is achieved by adjusting the ZMP within a current support envelope by applying joint torques that effectively modulate the foot-ground pressure field. The support envelope may also be adjusted, by stepping for example. The moment strategy involves performing motions with the head, trunk, arms and legs that generate CM moment such that the CMP diverges from the ZMP.

We used a humanoid model to test the MEC. This model, shown in Fig. 2, is human-like in form, and is 3-dimensional. The model has 7 segments: two feet, two lower leg segments, two upper leg segments, and a body segment that lumps the torso, head, and arms. The leg and body segments are modeled as cylinders, whereas the feet are modeled as rectangular blocks. Segment dimensions and masses are given in Table I, and in [24]. Twelve degrees of freedom correspond to joints (6 in each leg), and 6 degrees of freedom correspond to upper body position and orientation. Each leg is modeled with a ball-and-socket hip joint (3 degrees of

TABLE I

MODEL SEGMENT MASSES AND DIMENSIONS

Segment	Mass (kg)	Length (m)	Radius (m)
Foot	1.56	0.2	NA
Lower leg	4.48	0.48	0.05
Upper leg	10.73	0.46	0.08
Upper body	70.65	0.64	0.18

TABLE II

OUTPUTS TO BE CONTROLLED

Index	Output
1	Posterior-anterior CM position
2	Medio-lateral CM position
3	Vertical CM position
4	Upper body roll angle
5	Upper body pitch angle
6	Upper body yaw angle
7	Posterior-anterior swing foot position
8	Medio-lateral swing foot position
9	Vertical swing foot position
10	Swing foot roll angle
11	Swing foot pitch angle
12	Swing foot yaw angle

freedom), a pin knee joint (one degree of freedom), and a saddle-type ankle joint (two degrees of freedom). Note that although the humanoid model presented here does not include independently moving arms, the model, and the MEC control architecture can be easily extended to include additional limbs or degrees of freedom.

The outputs to be controlled are listed in Table II. These outputs are values relevant to balance control and locomotion, such as CM position, upper body orientation, and stepping foot position. Thus, the purpose of the MEC is to move the joints to achieve a desired motion for these outputs.

We specify desired motion behavior for the outputs using a linear proportional-differential (PD) control law:

$$\ddot{y_1} = k_s \left(y_{1set} - y_1 \right) + k_d \left(\dot{y_{1set}} - \dot{y_1} \right) \tag{4}$$

where y_1 is an output value to be controlled, y_{1set} and $\dot{y_{1set}}$ are position and velocity setpoints, and k_s and k_d are spring and damping gains. Such a control law can be represented as a set of virtual spring-damper elements

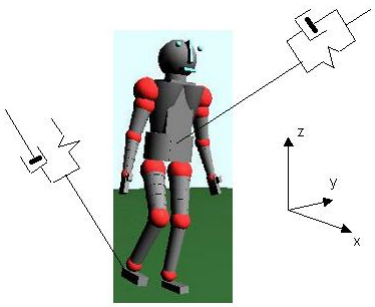

Fig. 2. Virtual linear spring-damper elements, attached to reaction points, allow the mechanism to be controlled as if it were a puppet.

attached to the output points being controlled, as shown in Fig. 2.

The MEC uses a model-based input-output linearization [22] to linearize and decouple the plant. This, by itself, is not sufficient because it is not always possible to achieve all control goals simultaneously. Actuation constraints, particularly, the requirement that the ZMP must remain well inside the support base in the case where foot roll is undesirable, may cause the overall system to become over-constrained, in which case some goals must be deferred. To address this problem, the MEC augments the input-output linearization with a slack variable relaxation technique to accommodate actuation constraints and prioritize goals. For example, the system may temporarily sacrifice goals of maintaining upright posture in order to achieve CM state goals.

A geometric transform, $\mathbf{h}$, is used to convert from the joint state to the workspace (output) state representation:

$$\mathbf{y} = \mathbf{h}\left(\mathbf{q}\right) \tag{5}$$

Differentiating this twice yields a relation between desired workspace acceleration, $\ddot{\mathbf{y}}_{des}$, and desired joint acceleration, $\ddot{\mathbf{q}}_{des}$:

$$\ddot{\mathbf{y}}_{des} = \mathbf{J}\ddot{\mathbf{q}}_{des} + \dot{\mathbf{J}}\dot{\mathbf{q}}_{des} \tag{6}$$

where $\mathbf{J}$ is the Jacobian. Note that 6 is linear for a given joint state. Also, because $\mathbf{y}$ and $\mathbf{q}$ are 12-element vectors, 6 represents a fully constrained system.

Inverse dynamics can now be used to compute desired joint torques corresponding to desired joint accelerations:

$$\mathbf{H}\left(\mathbf{q}\right)\ddot{\mathbf{q}}_{des} + \mathbf{C}\left(\mathbf{q}, \dot{\mathbf{q}}\right) + \mathbf{g}\left(\mathbf{q}\right) = \mathbf{T} \tag{7}$$

Combining 6 and 7 yields

$$\begin{bmatrix} \mathbf{I}_{12x12} & \mathbf{0}_{12x12} & \mathbf{0}_{12x12} \\ \mathbf{I}_{12x12} & -\mathbf{J} & \mathbf{0}_{12x12} \\ \mathbf{0}_{12x12} & \mathbf{H} & -\mathbf{I}_{12x12} \end{bmatrix} \begin{bmatrix} \ddot{\mathbf{y}} \\ \ddot{\mathbf{q}} \\ \mathbf{T} \end{bmatrix} = \begin{bmatrix} \ddot{\mathbf{y}}_{des} \\ \dot{\mathbf{J}}\dot{\mathbf{q}}_{des} \\ -\mathbf{C} \end{bmatrix} \tag{8}$$

Note that this is a fully constrained, linear system. The linearization is subverted if inequality constraints are introduced, and these constraints become active; the system becomes over-constrained in this case. An important constraint of this type is the requirement to keep the stance foot flat on the ground during single support because, while balancing on one leg it is undesirable for the stance foot to roll, particularly on its lateral edge. If the ZMP is on the edge of the support envelope, the foot may begin to roll [21]. Hence, in order to avoid foot roll, we employ linear inequality constraints to keep the ZMP inside the edge of the support envelope.

The ZMP for the humanoid model is obtained by expanding 1:

$$x_{ZMP} = \frac{\sum_{i=1}^{7} m_i r_{xi} \left(\ddot{r_{zi}} + g\right) - \sum_{i=1}^{7} m_i r_{zi} \ddot{r_{xi}} - \sum_{i=1}^{7} \tau_{yi}}{\sum_{i=1}^{7} m_i \left(\ddot{r_{zi}} + g\right)}$$

$$y_{ZMP} = \frac{\sum_{i=1}^{7} m_i r_{yi} \left(\ddot{r_{zi}} + g\right) - \sum_{i=1}^{7} m_i r_{zi} \ddot{r_{yi}} + \sum_{i=1}^{7} \tau_{xi}}{\sum_{i=1}^{7} m_i \left(\ddot{r_{zi}} + g\right)}$$

$$\tau_{xi} = I_{Gi}\dot{\omega_{xi}}, \tau_{yi} = I_{Gi}\dot{\omega_{yi}} \quad (9)$$

where i is the segment index; r_{xi}, r_{yi}, and r_{zi} denote the CM position of segment i; I_{Gi} is the inertia of segment i; and ω_{xi} and ω_{yi} are the angular velocities of segment i about the x and y axes. The moments τ_{xi} and τ_{yi} are about the segment i CM in the x and y directions. Equation 9 is is transformed into a set of linear inequality constraints by replacing x_{ZMP} and y_{ZMP} with min and max terms reflecting the bounds, so that these become constants.

$$\mathbf{H}_r \ddot{\mathbf{y}}_r \leq \mathbf{K}_r \quad (10)$$

where

$$\mathbf{H}_r = \begin{bmatrix} -\mathbf{m}^T \bullet \mathbf{r}_z^T & \mathbf{0}_{1x7} & \mathbf{x}_{max} & \mathbf{0}_{1x7} & -\mathbf{I}_y \\ \mathbf{m}^T \bullet \mathbf{r}_z^T & \mathbf{0}_{1x7} & \mathbf{x}_{min} & \mathbf{0}_{1x7} & \mathbf{I}_y \\ \mathbf{0}_{1x7} & -\mathbf{m}^T \bullet \mathbf{r}_z^T & \mathbf{y}_{max} & \mathbf{I}_x & \mathbf{0}_{1x7} \\ \mathbf{0}_{1x7} & \mathbf{m}^T \bullet \mathbf{r}_z^T & \mathbf{y}_{min} & -\mathbf{I}_x & \mathbf{0}_{1x7} \end{bmatrix}$$

$$\ddot{\mathbf{y}}_r = \begin{bmatrix} \ddot{\mathbf{r}}_x^T & \ddot{\mathbf{r}}_y^T & \ddot{\mathbf{r}}_z^T & \dot{\omega}_x^T & \dot{\omega}_y^T \end{bmatrix}$$

$$\mathbf{K}_r = \begin{bmatrix} g\left(m_{tot} x_{zmpmax} - \mathbf{m}^T \bullet \mathbf{r}_x^T\right) \\ -g\left(m_{tot} x_{zmpmin} - \mathbf{m}^T \bullet \mathbf{r}_x^T\right) \\ g\left(m_{tot} y_{zmpmax} - \mathbf{m}^T \bullet \mathbf{r}_y^T\right) \\ -g\left(m_{tot} y_{zmpmin} - \mathbf{m}^T \bullet \mathbf{r}_y^T\right) \end{bmatrix}$$

$$\mathbf{x}_{max} = \left(-x_{zmpmax}\mathbf{m}^T + \mathbf{m}^T \bullet \mathbf{r}_x^T\right)$$

$$\mathbf{x}_{min} = \left(x_{zmpmin}\mathbf{m}^T - \mathbf{m}^T \bullet \mathbf{r}_x^T\right)$$

$$\mathbf{y}_{max} = -\left(y_{zmpmax}\mathbf{m}^T + \mathbf{m}^T \bullet \mathbf{r}_y^T\right)$$

$$\mathbf{y}_{min} = \left(y_{zmpmin}\mathbf{m}^T - \mathbf{m}^T \bullet \mathbf{r}_y^T\right)$$

and $\mathbf{m}$ is a 7-element vector of masses for segments 1-7, $\mathbf{r}_x$, $\mathbf{r}_y$, and $\mathbf{r}_z$ are 7-element vectors of the segments' CM x, y, and z positions, $\mathbf{I}_x$ and $\mathbf{I}_y$ are 7-element vectors of the segments' inertias about the x and y axes, and x_{zmpmin}, x_{zmpmax}, y_{zmpmin}, and y_{zmpmax} are the ZMP limits. The operator $\bullet$ represents element-wise multiplication.

Inequality 10 is linear with respect to the current joint state. Furthermore, $\ddot{\mathbf{y}}_r$ is related to the joint acceleration vector through a linear function similar to 6. Therefore, if we combine the inequality constraints of 10 with 8, we have an overall system that is either fully constrained or over constrained.

We resolve the infeasibility of the over constrained case by artificially introducing flexibility in the form of "slack" variables [25]. The slack variable vector, $\ddot{\mathbf{y}}_{slack}$, has the same length as $\ddot{\mathbf{y}}$ (12 elements), and is introduced into 10 resulting in

$$\begin{bmatrix} \mathbf{I}_{12x12} & \mathbf{0}_{12x12} & \mathbf{0}_{12x12} & \mathbf{I}_{12x12} \\ \mathbf{I}_{12x12} & -\mathbf{J} & \mathbf{0}_{12x12} & \mathbf{0}_{12x12} \\ \mathbf{0}_{12x12} & \mathbf{H} & -\mathbf{I}_{12x12} & \mathbf{0}_{12x12} \end{bmatrix} \begin{bmatrix} \ddot{\mathbf{y}} \\ \ddot{\mathbf{q}} \\ \mathbf{T} \\ \ddot{\mathbf{y}}_{slack} \end{bmatrix} = \begin{bmatrix} \ddot{\mathbf{y}}_{des} \\ \dot{\mathbf{J}}\dot{\mathbf{q}}_{des} \\ -\mathbf{C} \end{bmatrix} \quad (11)$$

This system is under-constrained; it has 12 more variables than constraints. Even if inequality constraints in 10 become active, there will always be a feasible solution.

The slack variables act as a "safety valve", by relaxing the constraints. The slack variables should be computed so that their absolute value is minimized; we would like to achieve the goal as closely as possible. Furthermore, we would like the system to favor setting some slack variables non-zero over others. In particular, we would like the system to favor goals of horizontal CM acceleration over goals of upright orientation. To accomplish this, we formulate a quadratic minimization problem (quadratic program) where the variables to be computed are $\ddot{\mathbf{y}}$, $\ddot{\mathbf{q}}$, $\mathbf{T}$, $\ddot{\mathbf{y}}_{slack}$, and $\ddot{\mathbf{y}}_r$, 11 represents the linear equality constraints, 10 represents the linear inequality constraints, and where the cost to be minimized is

$$c = \sum \ddot{\mathbf{y}}_{slack}^T \mathbf{W} \ddot{\mathbf{y}}_{slack} \quad (12)$$

Here, $\mathbf{W}$ is a diagonal weighting matrix, where the diagonal elements are the costs associated with each slack variable. The costs for the slack variables for horizontal CM movement are higher than the costs for the slack variables for angular movement. Hence, setting the former to non-zero is more expensive than setting the latter to non-zero; it is more expensive to relax the goals for horizontal CM movement than the ones for upright orientation. The exact values of the weighting matrix elements are less important than their relative values; good performance is achieved over a wide range of values as long as the slack variable costs for horizontal movement are higher than those for angular movement. We solve the quadratic program using a standard quadratic program solver.

To compare the dynamical behavior of each model with that of human test participants, we performed a preliminary study of human motion in a balance situation similar to that used to evaluate the bipedal models. Kinetic and kinematic data were collected at the Holodeck Gait Laboratory of the Computer Science and Artificial Intelligence Lab at MIT. Three healthy male adult participants volunteered for the study. For this pilot investigation, each participant was asked to stand on his left foot, and lean to his left until his shoulder touched a support. The support was a flat force sensor, and the participant was asked to lean until this sensor measured approximately 20 N of force. This level of force corresponded to a leaning posture where the CM projection on the ground surface fell outside the stance foot envelope. The support was then suddenly pulled away. For each study participant, a total of ten trials were collected.

An infrared camera system (VICON 512) was used to measure the three-dimensional locations of reflective markers at 120 frames per second. A total of thirty-three markers were placed on various parts of a participant's body [17]. The VICON system was able to detect marker position with a precision of 1mm. Ground reaction forces were measured synchronously with the kinematic data at a sampling rate of 120 Hz using a force platform (Advanced Mechanical Technology Inc., Watertown, MA). The platforms measured ground reaction force and ZMP location at a precision of 0.1 N and 2mm, respectively.

Whole body CM position was computed from the kinematic data as described in [17]. The CMP location, CM moment, as well as moment and zero-moment horizontal forces were computed from the CM position, the ZMP, and the ground reaction force obtained from the force plate.

IV. Results

The model's CM controllability was tested by starting the humanoid in a motionless position, but with the medio-lateral CM position outside the support envelope. For such an initial condition, the zero-moment strategy is insufficient for restoring the CM over the stance foot, because the ZMP cannot be placed beyond the support envelope.

Fig. 3 shows the humanoid model's response to this initial system state. The clockwise rotation of the upper body and right swing leg results in moment about the CM that helps to move the medio-lateral CM position in the desired direction. As shown in Fig. 3A, the CM position begins outside the support envelope, but moves towards zero. The zero-moment force (black dashed line in Fig. 3D) is initially positive because the CM position is greater than the maximum allowable ZMP. This positive force is not desirable since it pushes the CM farther away from zero. Without the use of moment force, the CM will accelerate away from zero, as shown by the dashed line in Fig. 3A. The biped will fall because it begins in an out of balance state. To avoid this, the moment generated force (dotted gray line in Fig. 3D.) initially has a large negative value, resulting in an initial overall negative medio-lateral force (solid line in Fig. 3D.). Thus, the negative restoring force resulting from the angular movement of the upper body and swing leg provides enough equivalent horizontal ground reaction force to move the CM in the desired direction.

The initial negative CM moment (Fig. 3B) results in a deviation of trunk orientation from its desired upright value. However, after about 0.5 seconds, the ZMP (Fig. 3C) is no longer located at the foot's edge. At this point, the CM is under control, and can be beneficially influenced by zero-moment force alone. The controller then turns its attention to correcting the angular deviation in trunk orientation by exerting a positive CM moment. Thus, the controller temporarily sacrifices goals of upright posture in favor of goals for CM movement.

The motion of the human test participants when the force support was suddenly removed was similar to that shown in

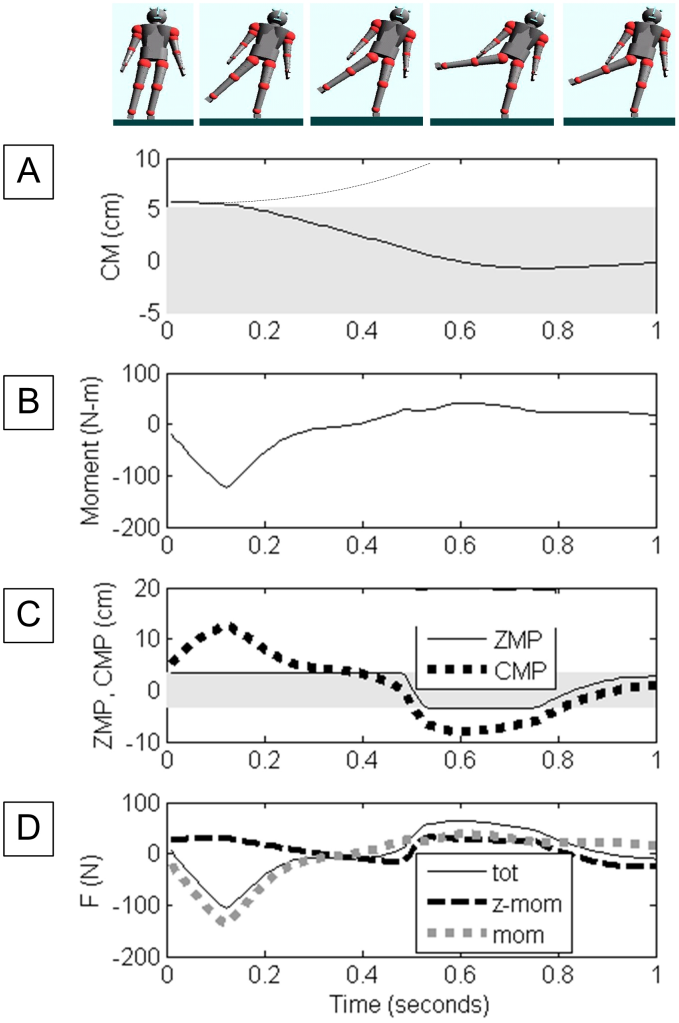

Fig. 3. Trajectories for the humanoid model disturbance test. In A), the medio-lateral CM ground projection (solid line) moves from beyond the outside edge of the support envelope, located at 5 cm, to the center of the stance foot, located at X = 0. The dotted line shows the trajectory if moment force is not used. In B), the moment about the CM is plotted. In C), the CMP (dotted line) departs from the ZMP (solid line) in regions of large CM moment. In D) the total medio-lateral force on the CM (solid line) consists of the zero-moment force (black dashed line) plus the moment force (dotted gray line).

Fig. 3. Fig. 4 shows trajectories resulting from a typical trial; results were consistent across participants and trials.

Similar to Fig. 4, the medio-lateral CM position, shown in Fig. 4a, begins slightly outside the boundary of the support envelope, which is at 5 cm, and then moves toward the center of the support envelope. Fig. 4b shows the moment about the CM. This value first goes negative, reaching a minimum of about -100 Nm after 200 ms, and then goes positive, reaching a maximum value of about 100 Nm after 700 ms. Fig. 4c shows the ZMP (solid line) and CMP (heavy dotted line) trajectories. Similar to Fig. 3, the CMP departs from the ZMP in order to exert additional medio-lateral force. Fig. 4d shows the total medio-lateral CM force (solid line), as well as

the component due to the zero-moment (black dashed line), and the component due to the moment (dotted gray line). The force component due to the moment dominates, reaching peaks of -100 and +100 N.

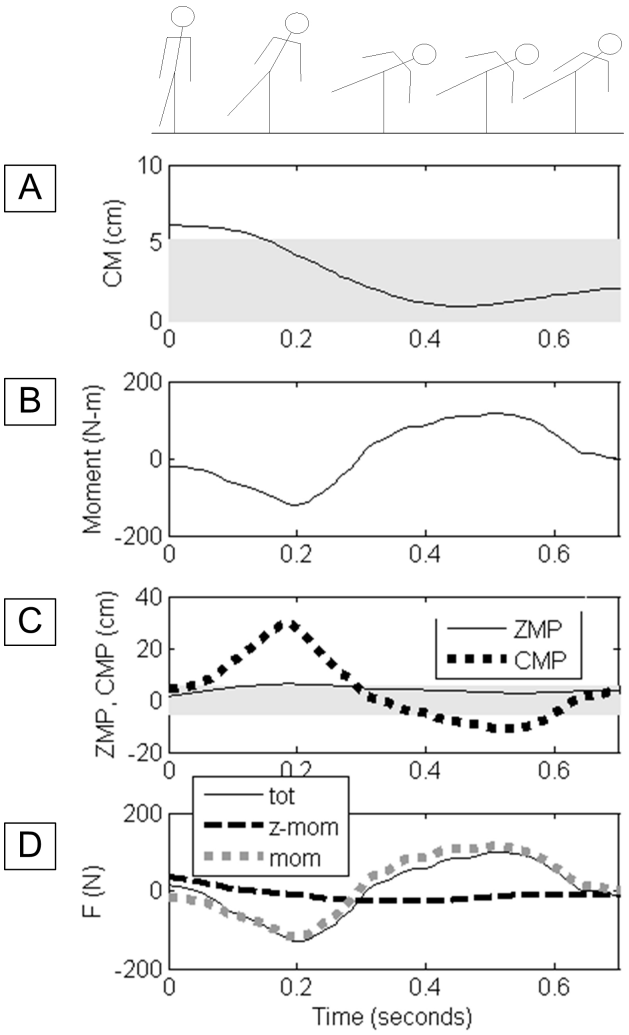

Fig. 4. Trajectories for a human balance test trial. In A), the medio-lateral CM position moves from beyond the outside edge of the support envelope (shown as shaded region) to the center. In B), the moment about the CM is first negative, reaching a minimum value of about -100 Nm, and then positive, reaching a maximum value of about 100 Nm. In C) the medio-lateral CMP (dotted line) departs from the medio-lateral ZMP (solid line), and moves outside the support base (shown as shaded region). In D), the total medio-lateral force on the CM (solid line) consists of the zero moment force (black dashed line) and the moment generated force (dotted gray line).

V. Discussion

In this study, we investigate movement tasks where bipedal balancing cannot be maintained using only a zero-moment, inverted pendulum control. We use a humanoid model to evaluate a Moment-Exploiting Control (MEC) algorithm that modulates whole-body angular momentum to enhance CM control.

As shown in Fig. 3, the MEC exhibits an improved capacity to regulate CM position and velocity in the presence of disturbances for single-leg balancing, by applying both zero-moment and moment CM force contribution. In contrast to previous controllers that use a ZMP reference trajectory, the MEC uses no such reference. However, the MEC does enforce the constraint that the ZMP remain within the support envelope so that the foot does not roll.

One challenge with using this type of approach is the reliance on model parameters, for example, the inertia matrix in 7. Addressing this problem is beyond the scope of this paper. One typical approach is to use feedback mechanisms, such as sliding mode control, to compensate for model error [19]. Further study is needed to determine the sensitivity of this approach to model parameters, and to determine the best methods for estimating these parameters.

References

[1] K. Hirai, "Current and Future Perspective of Honda Humanoid Robot," Proceedings of the 1997 IEEE/RSJ International Conference on Intelligent Robots and Systems, Grenoble, France, 1997, pp. 500 - 508.

[2] K. Hirai, M. Hirose, Y. Haikawa, and T. Takenaka, "The development of the Honda humanoid robot", IEEE International Conference on Robotics and Automation, 1998.

[3] J. Yamaguchi, E. Soga, S Inoue, and A. Takanishi, "Development of a bipedal humanoid robot - control method of whole-body cooperative dynamic biped walking", IEEE International Conference on Robotics and Automation, 1999.

[4] K. Nagasaka, M. Inaba, and H. Inoue. "Walking Pattern Generation for a Humanoid Robot Based on Optimal Gradient Method", IEEE International Conference on Systems, Man, and Cybernetics, pp. VI-908-913, 1999.

[5] M. Vukobratovic, and J. Stepanenko. "On the Stability of Anthropomorphic System". Mathematical Biosciences 15:1-37, 1972

[6] K. Nisiwaki, S. Kogami, Y. Kuniyoshi, M. Inaba, and H. Inoue, "Online Generation of Humanoid Walking Motion based on a Fast Generation Method of Motion Pattern that follows Desired ZMP," Proc. Of the IEEE/RSJ Intl. Conference on Intelligent Robots and Systems, pp. 2684-2688, 2002

[7] Y. Fujimoto and A. Kawamura. "Simulation of an Autonomous Biped Walking Robot Including Environmental Force Interaction." IEEE Robotics and Automation Magazine, 5(2):33-41, 1998

[8] S. Kagami, F. Kanehiro, Y. Tamiya, M. Inaba, and H. Inoue, "Autobalancer: an online dynamic balance compensation scheme for humanoid robots", Robotics: The Algorithmic Perspective, B. R. Donald, K. M. Lynch, D. Rus, editors, A. K. Peters Ltd.., 2001, pp. 329 - 340.

[9] T. Sugihara, Y. Nakamura, and H. Inoue, "Real-time Humanoid Motion Generation through ZMP Manipulation based on Inverted Pendulum Control," Proc. Of the IEEE International Conference on Robotics and Automation, pp. 1404-1409, 2002.

[10] S. Kajita, F. Kanehiro, K. Kaneko, K. Fujiwara, K. Harada, K. Yokoi, H. Hirukawa. "Resolved momentum control: humanoid motion planning based on the linear and angular momentum," Proceedings of the IEEE/RSJ International Conference on Intelligent Robots and Systems (IROS-2003), Las Vegas, Nevada, October 2003.

[11] S. Kajita, T. Nagasaki, K. Kaneko, K. Yokoi. "A hop towards running humanoid biped," IROS, 2004.

[12] T. Nagasaki, S. Kajita, K. Yokoi, K. Kaneko. "Running pattern generation and its evaluation using a realistic humanoid model," IEEE International Conference on Robotics and Automation, 2003.

[13] K. Ahn, Y. Oh. "Walking Control of a Humanoid Robot via Explicit and Stable CoM Manipulation with the Angular Momentum Resolution," IROS, 2006.

[14] A. Sano, J Furushu. "Realization of Natural Dynamic Walking Using the Angular Momentum Information, " ICRA, 1990.

[15] Z. Chi, M. Okamura, A. Kawamura, Y. Tomizawa. "Experimental approach for high speed walking of biped robot MARI, " Proc. of the 8th IEEE AMC, 2004.

[16] Popovic M., Hofmann A., Herr H. Angular Momentum Regulation during Human Walking: Biomechanics and Control. International Conference on Robotics and Automation; 2004 April; New Orleans, LA; pp.123-128.

[17] H. Herr, and M. Popovic, "Angular momentum in human walking", Journal of Experimental Biology. 211: 467-481, 2008.

[18] M. Popovic, A. Hofmann, H. Herr. "Zero spin angular momentum control: definition and applicability," IEEE RAS/RSJ International Conference on Humanoid Robots, Los Angeles (CA, USA). 2004.
[19] A. G. Hofmann, S. Massaquoi, M. Popovic, and H. Herr. "A sliding controller for bipedal balancing using integrated movement of contact and non-contact limbs." Proc. International Conference on Intelligent Robots and Systems (IROS). Sendai, Japan, 2004.
[20] A. G. Hofmann, "Robust Execution of Bipedal Walking Tasks From Biomechanical Principles," Ph.D. Thesis, Massachusetts Institute of Technology, 2005.
[21] M. Popovic, A. Goswami, and H. Herr, "Ground Reference Points in Legged Locomotion: Definitions, Biological Trajectories, and Control Implications," International Journal of Robotics Research, 2005.
[22] J. Slotine and W. Li. Applied Nonlinear Control. Ch. 6, Prentice Hall, NJ, USA
[23] O. Khatib, L. Sentis, J. Park, J. Warren. International Journal of Humanoid Robotics, 1(1):1-15, March 2004
[24] A. G. Hofmann, M. Popovic, H. Herr. Humanoid Standing Control: Learning from Human Demonstration. Journal of Automatic Control, 12(1), 16-22, 2002
[25] W. Wojsznis, T. Blevins, M. Nixon, P. Wojsznis. "Infeasibility Handling in MPC with Prioritized Constraints
[26] S. Kudoh, T. Komura and K. Ikeuchi. "The Dynamic Postural Adjustment with the Quadratic Programming Method", Proceedings of the 2002 IEEE/RSJ International Conference on Intelligent Robots and Systems, pp.2563-2568, 2002.